Article

Plasma-Based CH$_4$ Conversion into Higher Hydrocarbons and H$_2$: Modeling to Reveal the Reaction Mechanisms of Different Plasma Sources

Stijn Heijkers,* Maryam Aghaei, and Annemie Bogaerts*

Read Online

ACCESS | Metrics & More | Article Recommendations | Supporting Information

ABSTRACT: Plasma is gaining interest for CH$_4$ conversion into higher hydrocarbons and H$_2$. However, the performance in terms of conversion and selectivity toward different hydrocarbons is different for different plasma types, and the underlying mechanisms are not yet fully understood. Therefore, we study here these mechanisms in different plasma sources, by means of a chemical kinetics model. The model is first validated by comparing the calculated conversions and hydrocarbon/H$_2$ selectivities with experimental results in these different plasma types and over a wide range of specific energy input (SEI) values. Our model predicts that vibrational−translational nonequilibrium is negligible in all CH$_4$ plasmas investigated, and instead, thermal conversion is important. Higher gas temperatures also lead to a more selective production of unsaturated hydrocarbons (mainly C$_2$H$_2$) due to neutral dissociation of CH$_4$ and subsequent dehydrogenation processes, while three-body recombination reactions into saturated hydrocarbons (mainly C$_2$H$_6$, but also higher hydrocarbons) are dominant in low temperature plasmas.
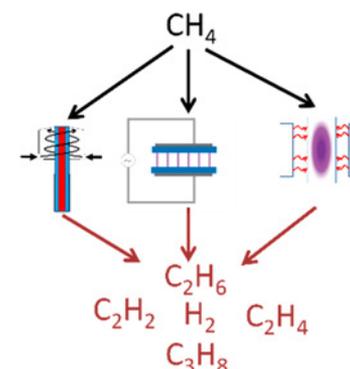
1. INTRODUCTION

The conversion of methane (CH$_4$) into higher hydrocarbons and H$_2$ is gaining interest as an alternative to steam reforming of crude-oil derivatives to form light olefins.[1] These olefins are the main building blocks in the chemical industry for fibers, synthetic rubbers, and other organic compounds.[2,3] Usually, CH$_4$ conversion is performed thermally, using high energy input and temperatures to activate the molecule.[4] Catalysts can make the process more efficient and/or selective, but catalyst instability due to carbon deposition is a major drawback.[2]

Plasma technology is gaining increasing interest for the nonoxidative conversion of CH$_4$, overcoming most of the drawbacks of thermal processes.[5] Plasma is created by applying electric energy to a gas. It is an ionized gas, consisting of various chemically active species (i.e., various types of radicals, ions, excited atoms and molecules, and electrons), besides the neutral gas molecules. The electrons in the plasma gain most of the applied electric energy, because of their small mass, and they activate the molecules by excitation, ionization, and dissociation, creating the above-mentioned reactive species, which can further react to form new molecules. This allows chemical conversions to occur at lower temperatures (even up to room temperature) than in thermal conditions.[5] Plasma is also very flexible and can easily be switched on/off, so it can use intermittent green electricity, which cannot be stored on the grid.[6]

Various types of plasma configurations have been applied already for CH$_4$ conversion, as summarized by Scapinello et al.[5] The most commonly used plasma types are dielectric barrier discharges (DBDs), microwave (MW), and gliding arc (GA)

plasmas. DBDs are created by applying an electric potential difference between two electrodes, of which at least one is covered by a dielectric barrier. They typically operate at (or slightly above) room temperature, and conversions were reported in the range between 1%[7] and 47%,[8] for a specific energy input (SEI, i.e., ratio of plasma power over gas flow rate) ranging between 0.1 and 300 kJ L^{-1}. Ethane (C$_2$H$_6$) is one of the main products formed, with selectivities ranging between 20%[8] and ca. 60%,[9] followed by the other C$_2$ hydrocarbons (i.e., ethylene (C$_2$H$_4$) and acetylene (C$_2$H$_2$)), C$_3$−C$_5$ compounds and soot. According to Scapinello et al.[5] the best overall result in a DBD, in terms of energy efficiency, conversion and product formation, was obtained by Xu and Tu,[10] with a CH$_4$ conversion of 11%, C$_2$H$_6$ selectivity of 34%, a selectivity of 19% for the other C$_2$ hydrocarbons, and the remainder being C$_3$−C$_4$ hydrocarbons and soot. These results were obtained at an SEI of 9 kJ L^{-1} (or 2.1 eV molec^{-1}), yielding a rather high energy cost for CH$_4$ conversion of 20 eV molec^{-1} and a low energy efficiency of 3.4%.

MW and GA plasmas operate at higher temperatures (typically 1000−3000 K), and are therefore called "warm plasmas".[6,11] They produce more unsaturated compounds, such

Table 1. Species Included in the Model

molecules	charged species	radicals	excited species
CH_4, H_2, C_2H_6, C_2H_4, C_2H_2, C_3H_8, C_3H_6, C_4H_{10}	CH_4^+, CH_5^+, CH_3^+, CH_2^+, CH^+, C_2^+, C^+, H^+, H_2^+, H_3^+, $C_2H_6^+$, $C_2H_5^+$, $C_2H_4^+$, $C_2H_3^+$, $C_2H_2^+$, C_2H^+ electrons	CH_3, CH_2, CH, C_2H, C_2, C, H, C_2H_5, C_2H_3, C_3H_7, C_3H_5, C_4H_9	CH_4(V1−V4), CH_4(J3, J4), H_2(V1−V14)

as C_2H_2. The conversions in MW plasmas range from 5% until above 90%,[12] at SEI values varying between 6.8 and 360 kJ L^{-1}.[12,13] The corresponding C_2H_2 selectivities vary from below 10%[12] until approximately 90%,[14] depending on the input power and gas pressure used, with higher pressures and/or powers producing more C_2H_2. The best result was obtained by Heintze and Magureaunu[12] at low pressure (30 mbar) and an SEI of 28 kJ L^{-1} (or 6.5 eV molec^{-1}), yielding a CH_4 conversion of 94%, an C_2H_2 selectivity of 65%, followed mainly by C_2H_4 (10%) and C_2H_6 (2%), and an energy cost of 6.9 eV molec^{-1} or energy efficiency of 23%.

Likewise, for GA plasmas, CH_4 conversions were reported from 0.2%[15] until 92%,[11] for SEI values between 2 and 42 kJ L^{-1},[11,16] and with C_2H_2 selectivities between 5%[17] and nearly 100%.[15] The best result was obtained by Polak,[18] reporting a CH_4 conversion of 86% and an C_2H_2 selectivity of 88%, followed by C_2H_4 (3%), at an SEI of 14 kJ L^{-1} (or 3.2 eV molec^{-1}). This resulted in a quite high energy efficiency of 49% and a low energy cost of 3.7 eV molec^{-1}.

Although the above plasma types show potential for CH_4 conversion into light olefins, only high power thermal arc discharges are up to now able to approach thermodynamic equilibrium conversions.[5,18] Therefore, more research is needed to improve the performance of the above plasma reactors. Specifically, we need to gain more knowledge on the most important reaction pathways in these kind of plasmas, to optimize the formation of higher hydrocarbons. Indeed, it is clear from the above that different plasma reactors yield very different hydrocarbon selectivities and CH_4 conversions, but the underlying reasons have not yet been studied in detail. A broad picture of possible pathways was presented by Scapinello et al.,[5] but to our knowledge, the importance of the different pathways in different reactors has not yet been clarified.

Therefore, in the present paper, we study the different reaction pathways of CH_4 conversion and (mainly) C_2 hydrocarbon and H_2 formation, using 0D chemical kinetics modeling, in the three most important plasma reactors discussed above.

A 0D chemical kinetics model is the most appropriate choice for describing a detailed plasma chemistry. In literature, some models have been presented already for CH_4 conversion in a DBD,[19−22] MW,[23] and GA plasma.[24] Also, CH_4/H_2 mixtures were modeled in moderate pressure MW plasmas, albeit for another application, i.e., plasma-assisted diamond deposition.[25,26] However, electron impact excitation of the internal degrees of freedom, such as vibrational and rotational excitation of CH_4, which might be important in warm plasmas (MW and GA plasmas) have not yet been taken into account into these plasma models. Moreover, a detailed comparison between the mechanisms in DBD, GA, and MW plasmas, based on such models, has not been performed yet. Hence, this will be the focus of the present paper.

2. MODEL DESCRIPTION

First, we will give a short outline of the 0D model and the chemistry used to describe CH_4 conversion, followed by explaining the assumptions made in the 0D approach to describe the different plasma reactors.

2.1. 0D Model Equations and Chemistry. The conservation eq 1 in a 0D model is solved for all species (see below):

$$\frac{\partial n_s}{\partial t} = \sum_{i=1}^{j} [(a_{s,i}^R - a_{s,i}^L)R_i] \tag{1}$$

where n_s is the density of species s (in cm^{-3}), j the total number of reactions in which that particular species is produced or consumed, $a_{s,i}^L$ and $a_{s,i}^R$ the stoichiometric coefficients at the left-hand side and right-hand side of a particular reaction equation, and R_i the rate of that reaction (in cm^{-3} s^{-1}), given by

$$R_i = k_i \prod_s n_s^{a_{s,i}} \tag{2}$$

where k_i is the rate constant (in cm^3 s^{-1} or cm^6 s^{-1} for two-body or three-body reactions, respectively) and $a_{s,i}$ was defined above.

The chemistry set applied in this study is based on the pure CH_4 chemistry part of the models developed by Snoeckx et al.[27] and Cleiren et al.,[28] extended with excitation and relaxation of the lowest vibrational and rotational levels. The set contains 57 different species (see Table 1), i.e., eight ground state molecules, 12 radicals, 16 ions, the electrons, six excited species of CH_4, and 14 of H_2. These species interact with each other through various chemical reactions. In total, 2174 reactions are included in our model, of which 378 are electron impact reaction, 380 are ionic reactions, 507 are neutral reactions, as well as 713 are vibration-translation (VT), and 196 are vibration-vibration (VV) relaxation reactions for CH_4 and H_2.

We solve this 0D model with the ZDPlaskin code.[29] The rate coefficients of the electron impact reactions are calculated from the corresponding energy-dependent cross sections and the electron energy distribution function, using the built-in Boltzmann solver BOLSIG+.[30] The rate coefficients of the other (i.e., heavy particle) reactions are adopted from literature. They are often a function of the gas temperature. Details of the CH_4 and H_2 vibrational levels and their reactions are given in the Supporting Information (SI, Table S.1). In addition, the full list of all the reactions and their corresponding rate coefficients, as well as the references of the cross sections used, are presented in Tables S.2−S.5 of the SI.

2.2. Modeling the Different Plasma Reactors with a 0D Approach. *2.2.1. General Aspects.* In all simulations, we made some general approximations, independent of the plasma reactor used:

1. Gas expansion can occur upon conversion of CH_4, e.g., when two new species are formed out of one, so we calculate the gas pressure and mass flow rate at every time step from the actual species densities, gas temperature, and velocity. To conserve the gas pressure and mass flow rate, the species densities (as calculated with the above conservation equations; see eq 1) and velocities are then corrected to account for this effect, following the method of Kozak and Bogaerts.[31]

2. The gas temperature is calculated self-consistently for the MW plasma in the same manner as done by Kozak and Bogaerts,[31] and a detailed description is given in the SI. For the DBD and the GA plasma, we adopt a temperature profile, as explained below.

3. A 0D model calculates the species densities as a function of time only, and neglects spatial variations. However, the time evolution can be translated into a spatial evolution (i.e., as a function of position in the plasma reactor) by means of the gas flow rate. In this way, local variations in the applied plasma power can be implemented in the model, as power pulses as a function of time (see details below).

4. The conversion of CH_4 is calculated as

$$\chi_{CH_4}(\%) = 100\% \frac{n_{CH_4,i}(cm^{-3})v_i(cm\ s^{-1}) - n_{CH_4,f}(cm^{-3})v_f(cm\ s^{-1})}{n_{CH_4,i}(cm^{-3})v_i(cm\ s^{-1})}$$

(3)

where $n_{CH_4 f}$ and $n_{CH_4 i}$ are the densities of CH_4 at the end and the beginning of the simulation, respectively, and v_f and v_i are the corresponding velocities.

5. The selectivities of the different hydrocarbons are calculated as

$$S_{C_xH_y}(\%) = 100\% \frac{x n_{C_xH_y}(cm^{-3})v_f(cm\ s^{-1})}{n_{CH_4,i}(cm^{-3})v_i(cm\ s^{-1}) - n_{CH_4,f}(cm^{-3})v_f(cm\ s^{-1})}$$

(4)

with $n_{C_xH_y}$ the density of the hydrocarbon. Note that these selectivities are C-based. We also define the H_2 selectivity, which is H-based:

$$S_{H_2}(\%) = 100\% \frac{0.5 n_{H_2}(cm^{-3})v_f(cm\ s^{-1})}{n_{CH_4,i}(cm^{-3})v_i(cm\ s^{-1}) - n_{CH_4,f}(cm^{-3})v_f(cm\ s^{-1})}$$

(5)

6. The specific energy input SEI deposited on the initial CH_4 flow is calculated as

$$SEI(kJ\ L^{-1}) = \frac{P(W)60(s\ min^{-1})}{\Phi(sccm)}$$

(6)

P is the deposited power in the plasma and Φ the flow rate. This SEI value can be converted into eV molec^{-1} as follows:[6]

$$SEI(eV\ molec^{-1}) = \frac{SEI(kJ\ L^{-1})6.24x10^{21}(eV\ kJ^{-1})24.5(L\ mol^{-1})p_0(101325\ Pa)}{6.022 \times 10^{23}(molec\ mol^{-1})p(Pa)}$$

(7)

with p_0 and p the atmospheric pressure and pressure inside the reactor, respectively. This allows us to calculate the energy cost for CH_4 conversion (either in kJ L^{-1} or eV molec^{-1}, depending on the unit of SEI):

$$EC = \frac{SEI \times 100\%}{\chi_{CH_4}(\%)\phi}$$

(8)

where ϕ is the fraction of CH_4 present in the feed gas.

2.2.2. Dielectric Barrier Discharge (DBD). As mentioned in the Introduction, a DBD is created by applying an electric potential difference between two electrodes, of which at least one is covered by a dielectric barrier. A DBD in CH_4 exhibits filamentary behavior, i.e., microdischarges between these electrodes. Hence, the CH_4 molecules will pass through several microdischarge filaments on their way throughout the reactor, which we mimic in the model as microdischarge power pulses as a function of time (cf. previous section). We applied our model to the DBD reactor of Xu and Tu[10] and to the micro-DBD reactor of Wang et al.,[32] in order to first verify our modeling results with their experiments, as a validation of our model. Indeed, these results are a good representation of other DBD reactor studies on CH_4 conversion, as reviewed by Scapinello et al.[5] Figure 1 illustrates a schematic picture of the cylindrical
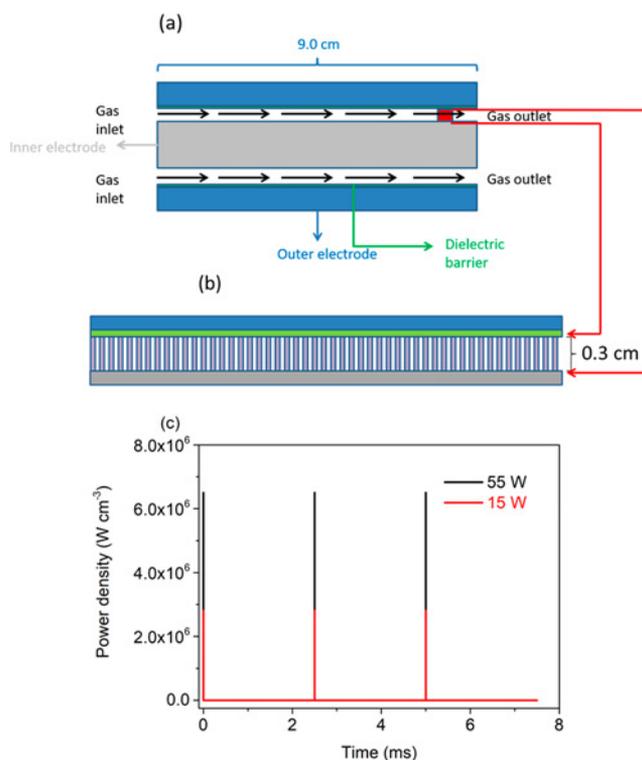
Figure 1. Schematic illustration of a typical cylindrical DBD reactor, based on the design of Xu and Tu[10] (a), representation of the filaments in this reactor (b), and the corresponding power density profile as a function of time in this DBD reactor, for three pulses, at an input power of 15 and 55 W and a frequency of the applied power of 20 kHz (c).

DBD reactor of Xu and Tu,[10] which has a length of 9 cm and a discharge gap of 0.3 cm, resulting in a discharge volume of 13.6 cm^3.[10] The micro-DBD reactor of Wang et al.[32] looks similar, but with a discharge gap of 0.09 cm, a length of 20 cm, and a discharge volume of 1.4 cm^3.

We assume that the plasma power is uniformly deposited in pulses (or microdischarges) with lifetimes of 11 ns for 15 W and 14 ns for 55W, based on linear interpolation of the micro-discharge lifetime as a function of power, adopted from Ozkan et al.[33,34] During one AC period in a DBD reactor, these authors measured approximately 400 microdischarges at 50 W and 500 microdischarges at 100 W, with an almost linear increase of the number of discharges as a function of power.[33] The local power deposition per pulse P_{pulse} (in W) is defined as

$$P_{pulse} = \frac{P_{total}}{N_{pulse}f_{AC}t_{pulse}}$$

(9)

where P_{total} (in W) is the global power input, which is varied between 15 and 55 W, based on the experiments of Xu and Tu,[10] and between 10 and 30 W for the experiments of Wang et al.,[32] N_{pulse} is the number of pulses per AC cycle, f_{AC} (in Hz) the frequency of the applied power, which is 20 kHz in our simulations, again based on Xu and Tu[10] and Wang et al.,[32] and t_{pulse} (in s) is the lifetime of the microdischarges (see above). Each of these microdischarges can be represented as a cylinder with a typical radius of ~0.13 mm[35,36] and a length equal to the discharge gap. Following Snoeckx et al.,[27,37] we assume that every molecule passes such a microdischarge every 100 half cycles, irrespective of power deposited. Detailed information on how the microdischarges are treated in the model, including the number of pulses per AC cycle and the temperature, is given in the SI.

2.2.3. Microwave (MW) Plasma. According to Scapinello et al.,[5] the majority of results for CH_4 conversion in MW plasmas were obtained by Heintze and Magureanu[12] at reduced pressure, and by Shen et al.[14] at atmospheric pressure. Both reactors are so-called surface wave MW plasmas, where microwave power is applied from the side, through a waveguide, to a cylindrical tube through which the gas flows (see schematic diagram in Figure 2).
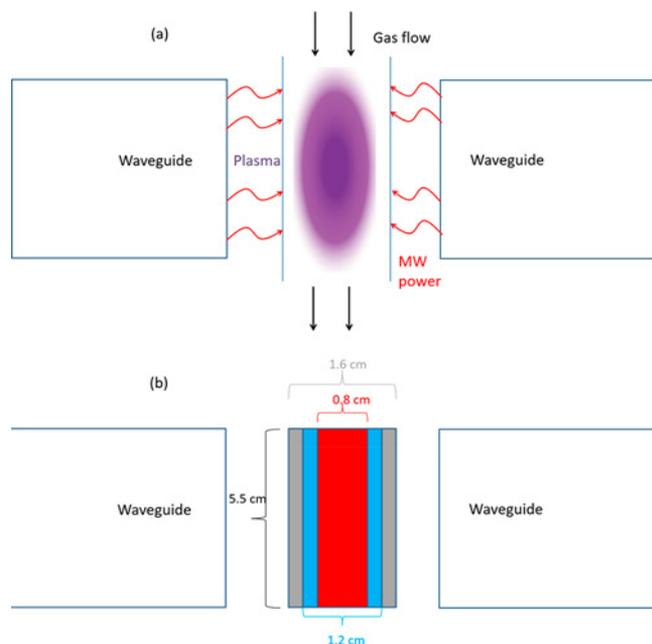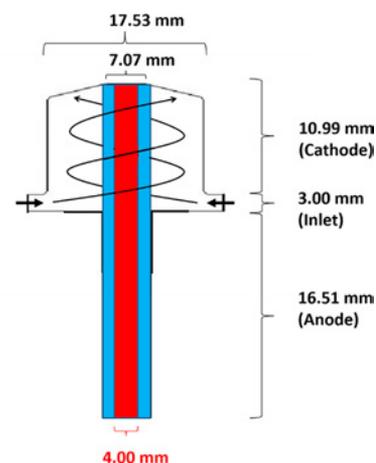

Figure 2. Schematic illustration of the atmospheric pressure MW plasma, based on the design of Shen et al.[14] (a) and its implementation in the 0D model (b). The arrows depict the direction of the gas flow and the different colors in (b) indicate the hot center (red) and cooler (blue and gray) zones (see text in SI).

Hence, we applied our model to the wide range of conditions in both studies, to validate our model. Details of both reactor configurations and discharge conditions, and the assumptions made in our model on power deposition and corresponding temperature in the plasma, are given in SI.

2.2.4. Gliding Arc (GA) Plasma. The results on GA performance, as reviewed by Scapinello et al.,[5] are quite scattered. A classical GA is formed between two flat converging electrodes, between which an electric potential difference is applied, creating an arc discharge, that glides along the electrodes under influence of the gas flow, toward rising interelectrode distance, until it extinguishes and a new arc is formed at the shortest interelectrode distance.[38] However, the residence time of the gas inside the arc plasma is quite limited in classical GA discharges. For this reason, a cylindrical GA discharge, also called gliding arc plasmatron (GAP), was developed by Nunnally et al.,[39,40] and showed promising results for CO_2 splitting[39–42] and dry reforming of CH_4.[28] Therefore, we performed experiments in this GAP for pure CH_4 conversion to validate our model. A schematic picture of this GAP configuration is given in Figure 3.

Figure 3. Schematic illustration of the GAP, with characteristic dimensions of cathode (reactor body), inlet region (insulator), anode (outlet) and arc region, and indication of the outer vortex (solid spiral). The inner (reverse) vortex is not depicted for the sake of clarity, but it is confined in the red and blue rectangles. The red rectangle shows the arc region, and the blue region is the hot region right next to it, inside the inner vortex.

It consists of a cylindrical reactor body (at cathode potential) and a reactor outlet (at anode potential). The gas flows in through six tangential inlets, creating a vortex flow. When the anode (= outlet) diameter is smaller than the cathode (= reactor body) diameter, the incoming gas will not immediately escape the reactor through the outlet at the bottom of the reactor, as it follows a vortex flow with larger diameter, so it will be forced upward in the cathodic part of the reactor, in a so-called forward vortex flow (FVF) pattern. When the spiraling gas arrives at the top of the reactor, the rotational speed will be reduced due to friction and inertia, and it will start to move downward in a smaller vortex, toward the outlet at the bottom, i.e., in a reverse vortex flow (RVF). The latter stabilizes the arc in the center of the reactor and it minimizes heat losses toward the walls. In this way, the residence time inside the arc is longer than in classical GA discharges, with a larger plasma volume. Therefore, the performance in terms of gas conversion is generally better than in classical GA discharges.

The arc plasma in a GAP is confined within the inner vortex and is more or less uniform, allowing a straightforward description of this GA configuration with our 0D model. Moreover, the arc dimensions change little with electric current, as investigated by Trenchev et al.[43,44] We assume that the arc has a diameter of 4 mm, as in our earlier simulations.[28,41,42,45] This corresponds to an arc volume of 383 mm³. Right next to the arc, there is still a warm zone until the edge of the inner vortex, where the temperature is still above 1000 K, and thus where thermal CH_4 conversion can still take place.[28]

In both the experiments and simulations, we did not use pure CH_4 as the latter did not allow plasma ignition in our GAP reactor. Therefore, we added between 80% and 50% N_2, and consequently, we expanded the chemistry in our model with N_2 and CH_4–N_2 chemistry, as explained in the SI. The power deposited inside the plasma was 224 W and the flow rate was 10 L min^{-1}. Based on earlier 3D fluid dynamics calculations by Trenchev et al.,[44] this corresponds to a velocity of 196 cm s^{-1} and a residence time of 15 ms. The SEI value is 1.3 kJ L^{-1}.

3. RESULTS AND DISCUSSION

In the following sections, we will always first compare the calculated CH_4 conversion and energy cost with experimental data, as well as the selectivities of the most important hydrocarbons (and H_2 when available), for a wide range of conditions, to verify whether the model predicts the right chemistry in each of the plasma sources. Subsequently, we can use the model to elucidate the underlying reaction pathways for CH_4 conversion into higher hydrocarbons and H_2, in DBD, MW, and GA plasmas. It should be noted that only C atom formation, but no solid carbon formation is included in our model, because we only describe the gas phase chemistry. Furthermore, it was stated in the experimental papers to be always below 10% in the DBD and MW plasma at atmospheric pressure,[10,14,32] while in the MW plasma at reduced pressure, it was also stated to be negligible in the pulsed mode.[12] In the MW plasma at reduced pressure in continuous mode and in our own GAP experiments, however, significant solid carbon formation was observed, so in the future, we should improve our model to account for it, by adding surface processes.

3.1. DBD Plasma. *3.1.1. Comparison of Calculated and Measured CH_4 Conversion, Energy Cost, and Product Selectivities.* The calculated and experimental results for CH_4 conversion, energy cost, and selectivities of the most important hydrocarbons and H_2 in the DBD reactor of Xu and Tu[10] are plotted as a function of flow rate and plasma power in Figures 4 and 5, respectively. The experimental and calculated data follow (more or less) the same trend with increasing flow rate. The largest discrepancies are seen for the selectivities of C_2H_6 and C_2H_2/C_2H_4, with maximum relative discrepancies of 62% for C_2H_6 at 50 mL min^{-1} and 53% for C_2H_4/C_2H_2 at 300 mL min^{-1} (see Figure 4). Also the trends as a function of plasma power are in reasonable agreement, except for the C_2H_6 selectivity, which decreases in our model, whereas the experiments indicate a small rise. The largest discrepancy for the C_2H_6 selectivity is however still only 31% (see Figure 5). The average discrepancy between the calculated and experimental results is 25%, which is satisfactory, in view of the complex chemistry and the assumptions made in the 0D model. Hence, we believe the model is able to elucidate the most important mechanisms in this DBD discharge.

The calculated and experimental conversions, energy costs and product selectivities for the DBD reactor of Wang et al.[32] are plotted in Figures 6 and 7, as a function of flow rate and plasma power, respectively. The H_2 selectivity was not measured as a function of flow rate, and therefore, only the calculated H_2 selectivities are shown in Figure 6. Again, the conversion, energy cost, and selectivities generally follow the same trends. Note that the energy cost is rather constant in the model, while the experimental values slightly drop as a function of flow rate (see Figure 6), but this is because the measured conversion drops more slowly than the calculated values at rising flow rate (and thus lower SEI). Indeed, when the flow rate rises by a factor 3
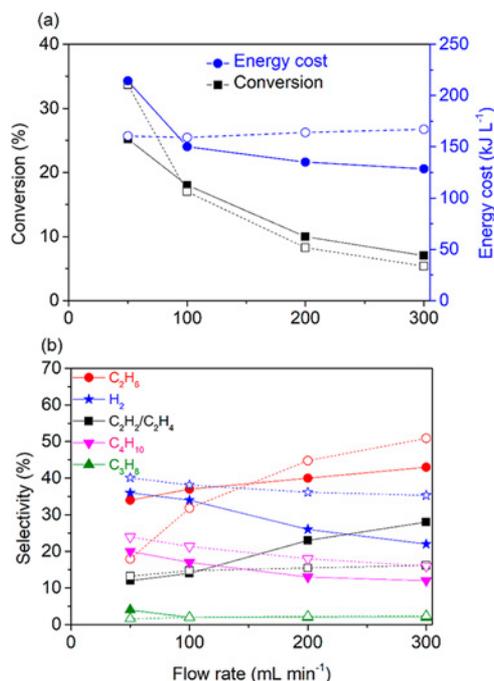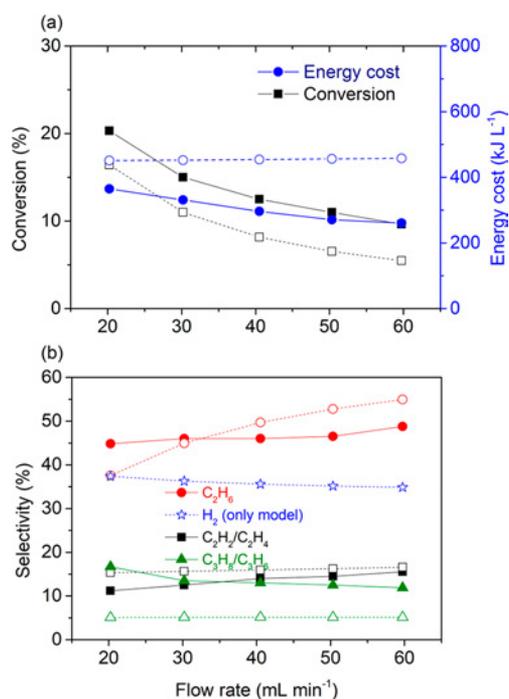

Figure 4. Calculated (dashed lines) and experimental (solid lines) CH_4 conversions and energy costs (a), as well as selectivities of the most important hydrocarbons and H_2 formed (b), as a function of flow rate, at a plasma power of 45 W in an atmospheric pressure DBD reactor. The experimental results are adopted from Xu and Tu.[10]
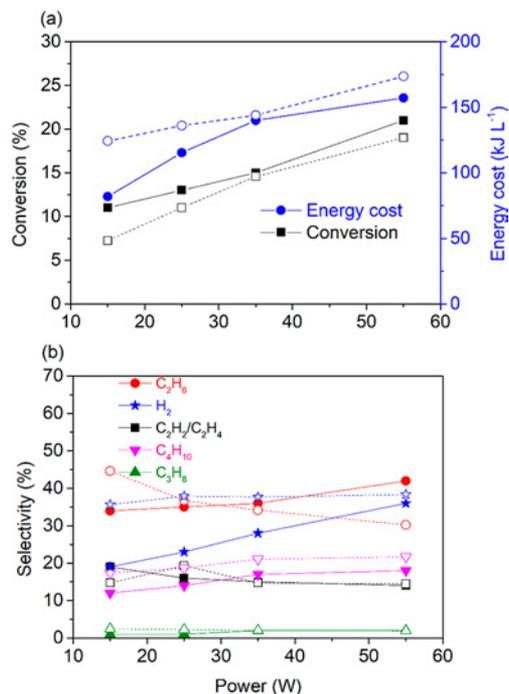
Figure 5. Calculated (dashed lines) and experimental (solid lines) CH_4 conversions and energy costs (a), as well as selectivities of the most important hydrocarbons and H_2 formed (b), as a function of plasma power, at a flow rate of 100 mL min^{-1} in an atmospheric pressure DBD reactor. The experimental results are adopted from Xu and Tu.[10]

(and thus, the SEI drops by a factor 3, at constant power), the calculated conversion drops by a factor 3 as well (thus explaining the constant energy cost), while the measured conversion only drops by a factor 2 (thus explaining why the energy cost slightly
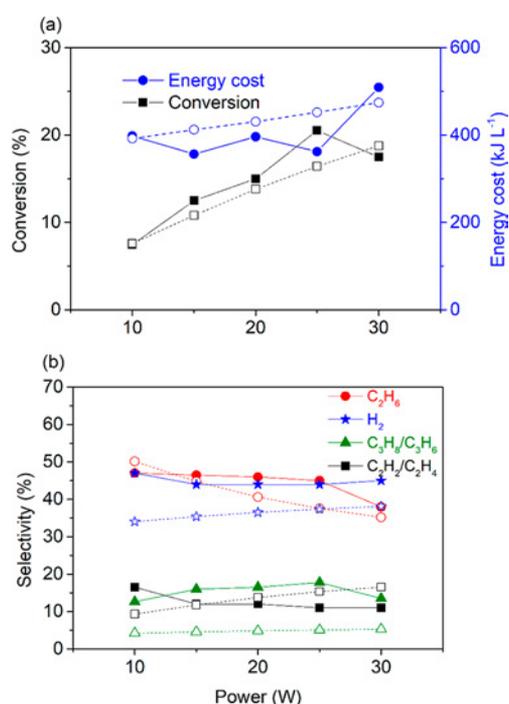
Figure 6. Calculated (dashed lines) and experimental (solid lines) CH_4 conversions and energy costs (a), as well as selectivities of the most important hydrocarbons and H_2 formed (b), as a function of flow rate, at a plasma power of 25 W in an atmospheric pressure DBD reactor. The experimental results are adopted from Wang et al.[32]


Figure 7. Calculated (dashed lines) and experimental (solid lines) CH_4 conversions and energy costs (a), as well as selectivities of the most important hydrocarbons and H_2 formed (b), as a function of plasma power, at a flow rate of 20.24 mL min^{-1} in an atmospheric pressure DBD reactor. The experimental results are adopted from Wang et al.[32]

drops). In addition, also the C_2H_2/C_2H_4 selectivities show some discrepancy, because the experimental data slightly drop and the calculation results slightly rise upon increasing plasma power

(see Figure 7). However, the maximum relative difference is about 50%, which is still reasonable, in view of the assumptions made in the 0D model. Also the absolute values of the calculated and experimental results are in satisfactory agreement, except for the C_3H_8/C_3H_6 selectivities, which exhibit a maximum discrepancy of 72% at a plasma power of 15 W and a flow rate of 20.2 mL min^{-1} (see Figure 7). The average discrepancy between the calculated and experimental results is 37%, which we believe is good enough for explaining the underlying chemistry in a DBD reactor.

In both reactors, the conversions vary between 7% and 21%, decreasing with rising flow rate and increasing with power. Based on the conditions used, this corresponds to energy costs varying between 82 kJ L^{-1} (or 19 eV molec^{-1}) at a plasma power of 15 W and a flow rate of 100 mL min^{-1} (i.e., SEI = 9 kJ L^{-1}, for the conditions of Xu and Tu;[10] Figure 5), up to 509 kJ L^{-1} (or 118 eV molec^{-1}) at a plasma power of 30 W and a flow rate of 20.2 mL min^{-1} (i.e., SEI = 89 kJ L^{-1}, for the conditions of Wang et al.;[32] see Figure 7). The average energy cost for CH_4 conversion for all conditions studied is 259 kJ L^{-1} (or 60 eV molec^{-1}), which is very high. Both in the model and experiments, C_2H_6 is by far the most important hydrocarbon, followed by C_2H_2 and C_2H_4, C_4H_{10}, and finally C_3H_8. Other (unsaturated or higher) hydrocarbons were not reported in both papers, but according to our model, C_5H_{12} can also be formed, and further polymerization toward C_6 and higher hydrocarbons is also possible. In addition, H_2 is formed in large amounts, both in the experiments and our model.

3.1.2. Underlying Reaction Pathways. The most important reactions in the DBD plasma are visualized in Figure 8. The thickness of the arrow lines is a measure for the importance of the reactions, determined by the reaction rates, as calculated in the model. These calculated rates are listed in the SI (Table S.6).
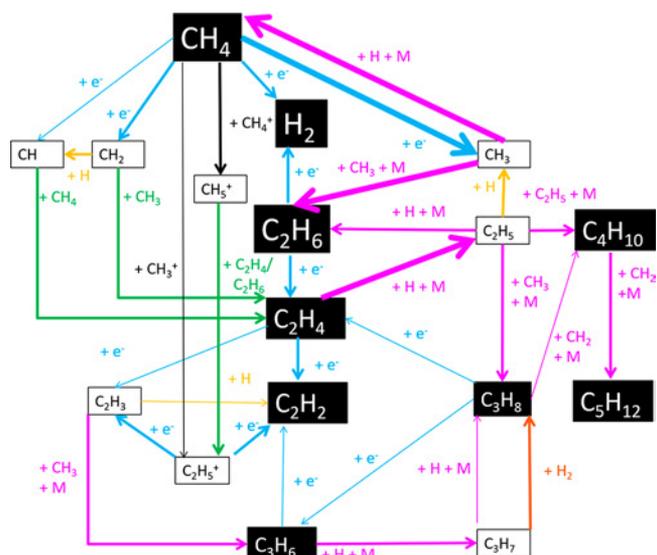
Figure 8. Most important net reaction pathways in a DBD at atmospheric pressure. Blue, pink, yellow, green, and orange arrow lines represent electron impact reactions, three-body reactions, two-body reactions with H atoms, reactions with hydrocarbon molecules or radicals, and two-body reactions with H_2, respectively. The thickness of the arrow lines is proportional to the reaction rate, while the size of the boxes is proportional to the species density, as calculated in the model. The black boxes represent stable molecules and the white boxes intermediates (radicals or ions).

CH_4 is mainly converted by electron impact dissociation into CH_3 radicals ($e^- + CH_4 \rightarrow e^- + CH_3 + H$), as well as into CH_2 and CH radicals ($e^- + CH_4 \rightarrow e^- + CH_2 + H_2$ and $e^- + CH_4 \rightarrow e^- + CH + H + H_2$). The dissociation into CH_2 and H_2 ($e^- + CH_4 \rightarrow e^- + CH_2 + H_2$) is one of the most important H_2 formation processes (together with $e^- + C_2H_6 \rightarrow e^- + C_2H_4 + H_2$; see below).

In addition, CH_4 undergoes electron impact ionization and dissociative ionization ($e^- + CH_4 \rightarrow e^- + e^- + CH_4^+$ and $e^- + CH_4 \rightarrow e^- + e^- + CH_3^+ + H$). The CH_4^+ and CH_3^+ ions formed in this way are not indicated as separate species in Figure 8, as they quickly react with CH_4, forming $C_2H_5^+$ ($CH_3^+ + CH_4 \rightarrow C_2H_5^+ + H_2$) or CH_5^+ ($CH_4^+ + CH_4 \rightarrow CH_5^+ + CH_3$).

The CH_3 radicals partially recombine with H ($CH_3 + H + M \rightarrow CH_4 + M$) forming again CH_4, but they also recombine with another CH_3 radical ($CH_3 + CH_3 + M \rightarrow C_2H_6 + M$) to form C_2H_6, which is the most important production mechanism of C_2H_6, and it occurs mainly in the microdischarge pulses of the DBD, where the CH_3 radicals as necessary building blocks are formed.

C_2H_6 is partially converted into C_2H_4, by electron impact dissociation ($e^- + C_2H_6 \rightarrow e^- + C_2H_4 + H_2$), which is the main population mechanism of C_2H_4 and one of the main population mechanisms of H_2 (cf. above). In addition, C_2H_4 is also formed upon (radical) recombination reactions ($CH_3 + CH_2 \rightarrow C_2H_4 + H$ and $CH_4 + CH \rightarrow C_2H_4 + H$).

C_2H_4 partially recombines with H into C_2H_5 ($C_2H_4 + H + M \rightarrow C_2H_5 + M$), and C_2H_5 recombines further with C_2H_5 into C_4H_{10} ($C_2H_5 + C_2H_5 + M \rightarrow C_4H_{10} + M$), as well as with H ($C_2H_5 + H \rightarrow CH_3 + CH_3$) forming again two CH_3 radicals, and with CH_3 ($CH_3 + C_2H_5 + M \rightarrow C_3H_8 + M$) forming C_3H_8. The latter reaction is however less important than the other two reactions, explaining why C_4H_{10} was formed in larger amounts than C_3H_6/C_3H_8 in the experiments of Xu and Tu[10] (see Figures 4 and 5). Moreover, C_2H_4 also undergoes electron impact dissociation ($e^- + C_2H_4 \rightarrow e^- + C_2H_2 + H_2$ and $e^- + C_2H_4 \rightarrow e^- + C_2H_3 + H$).

In addition, C_2H_4 and C_2H_6 react with CH_5^+ ions, forming $C_2H_5^+$ ($CH_5^+ + C_2H_6 \rightarrow C_2H_5^+ + H_2 + CH_4$ and $CH_5^+ + C_2H_4 \rightarrow C_2H_5^+ + CH_4$). $C_2H_5^+$ is an important intermediate for the formation of C_2H_2 and C_2H_3, by dissociative recombination with electrons ($e^- + C_2H_5^+ \rightarrow C_2H_3 + H + H$, $e^- + C_2H_5^+ \rightarrow C_2H_2 + H_2 + H$, and $e^- + C_2H_5^+ \rightarrow C_2H_2 + H + H + H$). The C_2H_3 radicals mainly recombine with CH_3 radicals into C_3H_6 ($CH_3 + C_2H_3 + M \rightarrow C_3H_6 + M$), as well as with H ($C_2H_3 + H \rightarrow C_2H_2 + H_2$) forming C_2H_2.

C_3H_6 undergoes electron impact dissociation into C_2H_2 ($e^- + C_3H_6 \rightarrow e^- + C_2H_2 + CH_4$), but it mainly recombines with H, forming C_3H_7 ($C_3H_6 + H + M \rightarrow C_3H_7 + M$). The latter radical quickly forms C_3H_8 upon reaction with H_2 ($C_3H_7 + H_2 \rightarrow C_3H_8 + H$), as well as by three-body recombination with H ($C_3H_7 + H + M \rightarrow C_3H_8 + M$).

C_3H_8 partially creates again C_3H_6 by electron impact dissociation ($e^- + C_3H_8 \rightarrow e^- + C_3H_6 + H_2$) or it recombines with CH_2 into C_4H_{10} ($C_3H_8 + CH_2 + M \rightarrow C_4H_{10} + M$). Finally, C_4H_{10} recombines with CH_2 radicals into C_5H_{12} ($C_4H_{10} + CH_2 + M \rightarrow C_5H_{12} + M$), which will further react into the formation of higher hydrocarbons by the same type of recombination reaction.

Hence it is clear that in a DBD electron impact dissociation processes are predominant. They create radicals, which mainly recombine with other radicals or H atoms, due to the lower temperatures, forming especially the saturated hydrocarbons, such as C_2H_6, C_3H_8, and C_4H_{10}.

3.2. MW Plasma. *3.2.1. Comparison of Calculated and Measured CH_4 Conversion, Energy Cost, and Product Selectivities.* The experimental and calculated CH_4 conversions, energy costs, and selectivities of the most important hydrocarbons are plotted as a function of SEI in Figures 9 and 10, for a
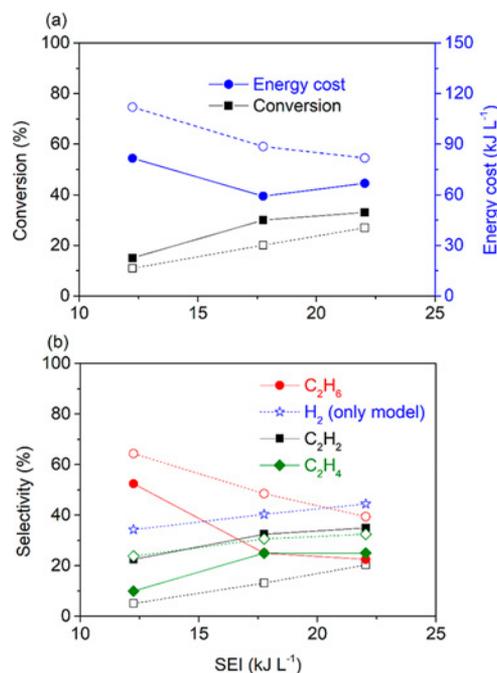
Figure 9. Calculated (dashed lines) and experimental (solid lines) CH_4 conversions and energy costs (a), as well as selectivities of the most important hydrocarbons and H_2 formed (b), as a function of SEI, in a MW plasma at a pressure of 30 mbar and flow rate of 98 sccm, operating in a continuous regime. The experimental results are adopted from Heintze and Magureaunu.[12]

MW discharge at reduced pressure, i.e., 30 mbar, for a continuous and a pulsed discharge, respectively. Again, no H_2 selectivities were reported in the experiments, so only the calculated values are given. In the pulsed regime, we also compare the calculated and measured gas temperature in Figure 10. Figures 11 and 12 show the experimental and calculated CH_4 conversions, energy costs, and most important product selectivities in a MW discharge at atmospheric pressure, as a function of power and flow rate, respectively. Note that these experiments were performed in a CH_4/H_2 mixture, so the H_2 selectivities could not be determined, since H_2 is also a reactant.

In general, the difference between the calculated and experimental results is higher for lower powers and reduced pressure than for higher pressures and higher powers. The C_2H_2 selectivities in the reduced pressure MW plasma in continuous mode show the largest discrepancies, even up to almost a factor of 5 (i.e., calculated C_2H_2 selectivity of 5% versus 23%, for an SEI value of 12 kJ L^{-1}). The reason is probably the underestimation of the gas temperature and the assumption that the power is evenly distributed over the whole radial distance of the reactor tube. In the atmospheric pressure MW plasma the largest discrepancies are found for the C_2H_4 selectivities, i.e., up to a factor of 6 (calculated C_2H_4 selectivity of 3% versus 18%, at 400 W and 500 mL min^{-1}; see Figure 11). Nevertheless, in both the reduced pressure and atmospheric pressure MW plasma the
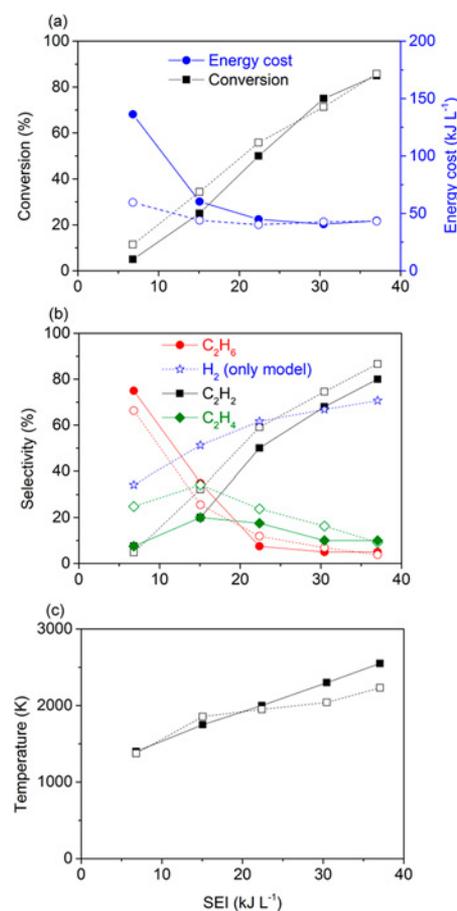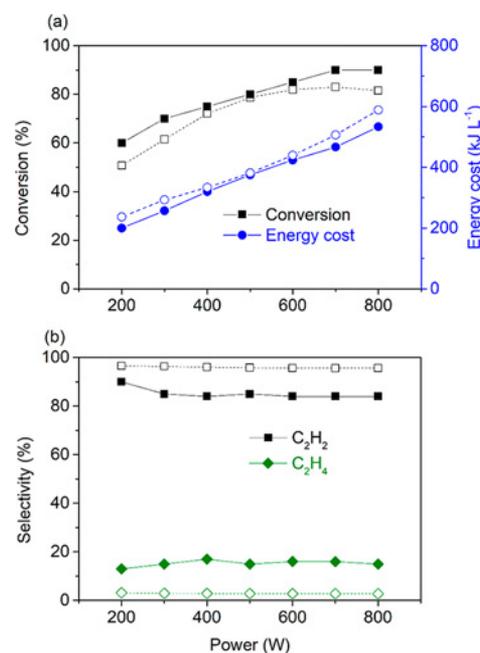
Figure 10. Calculated (dashed lines) and experimental (solid lines) CH_4 conversions and energy costs (a), as well as selectivities of the most important hydrocarbons and H_2 (b), and gas temperatures (c), as a function of SEI, in a MW plasma at a pressure of 30 mbar and flow rate of 98 sccm, operating in a pulsed regime. The experimental results are adopted from Heintze and Magureaunu.[12]

Figure 11. Calculated (dashed lines) and experimental (solid lines) CH_4 conversions and energy costs (a), as well as selectivities of C_2H_4 and C_2H_2 (b), as a function of microwave power, at a flow rate of 500 mL min^{-1} in an atmospheric pressure MW plasma, for a CH_4/H_2 ratio of 1/4. The experimental results are adopted from Shen et al.[14]

Figure 12. Calculated (dashed lines) and experimental (solid lines) CH_4 conversions and energy costs (a), as well as selectivities of C_2H_4 and C_2H_2 (b), as a function of flow rate, at a microwave power of 400 W in an atmospheric pressure MW plasma, for a CH_4/H_2 ratio of 1/4. The experimental results are adopted from Shen et al.[14]
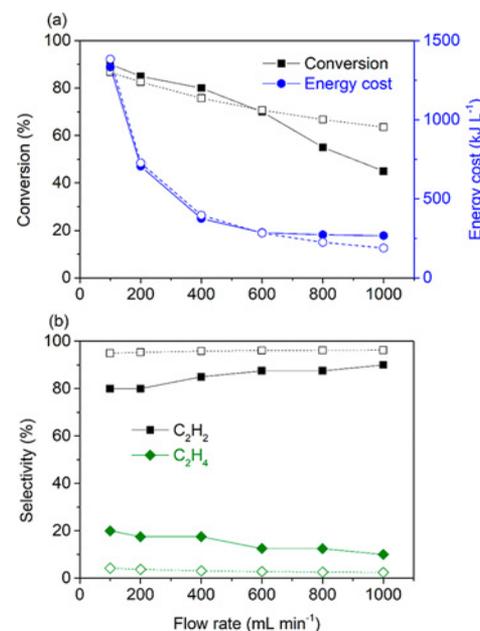
experimental and calculated results show the same trend and on average the discrepancy between calculated and experimental results is 40% for the reduced pressure MW plasma and 44% for the atmospheric pressure plasma. In addition, the difference between calculated and measured gas temperature in the pulsed reduced pressure MW plasma is less than 12%, so we believe that a qualitative description of the reaction mechanisms in MW plasmas operating in different pressure regimes is feasible with our model and will be presented in the next section.

It is clear that the CH_4 conversion in the MW plasma, both at reduced and atmospheric pressure, can reach values above 80%, for high power and low flow rate or high SEI values. The energy costs range from about 50 to above 100 kJ L^{-1} at reduced pressure, which is lower than in a DBD. In the atmospheric pressure MW plasma, the energy costs vary from 200 to above 1000 kJ L^{-1}, which is of the same order or even higher than in the DBD. However, it should be mentioned that the gas flow in this case was diluted with H_2, (CH_4/H_2 ratio of 1/4), which reacts to a large extent with the dissociation products of CH_4, forming again CH_4. This means that not all of the power is efficiently used for CH_4 conversion, explaining the higher energy cost.

For lower power and pressure, the main products formed are C_2H_6 (with selectivities ranging between 5% and 75%), C_2H_4 (with selectivities ranging from 8% to 20%), and C_2H_2 (with selectivities ranging from 8% to 80%). Higher hydrocarbons,

such as created in the DBD, were not observed in our model, and also not reported experimentally. This is attributed to the high temperatures in the MW plasma (above 1000 K), which will cause dissociation of these higher hydrocarbons back in smaller compounds. Furthermore, the higher the SEI value, the larger the shift toward C_2H_2 and C_2H_4, instead of C_2H_6. At atmospheric pressure, CH_4 is mainly converted into C_2H_2

with a selectivity of ∼85%, and to C_2H_4 with a selectivity of ∼15%. Although different conditions give different product selectivities, especially at reduced pressure, we can draw an overall picture of the most important mechanisms at reduced pressure vs atmospheric pressure, as outlined in next section.

3.2.2. Underlying Reaction Pathways. It is clear from above that the different pressure regimes in a MW plasma show different product distributions, which are attributed to different mechanisms, as can be seen in Figures 13 and 14. Again, the
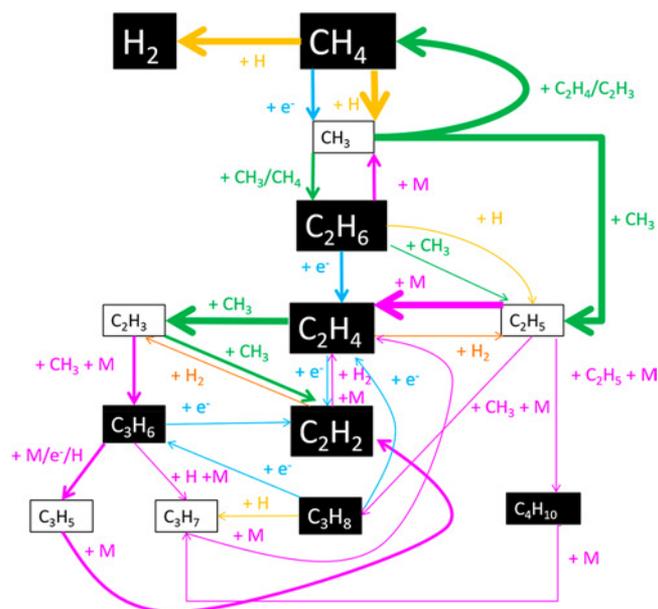
Figure 13. Most important net reaction pathways in a MW plasma at reduced pressure. Blue, pink, yellow, green, and orange arrow lines represent electron impact reactions, reactions involving a neutral species M in three-body reactions or neutral dissociation, two-body reactions with H atoms, two-body reactions with hydrocarbon molecules or radicals, and with H_2 molecules, respectively. The thickness of the arrow lines and the size of the boxes are proportional to the reaction rate and species density, respectively, as calculated in the model. The black boxes represent stable molecules and the white boxes intermediates (radicals).

thickness of the arrow lines are a measure for the importance of the reactions, determined by the reaction rates, as calculated in the model. These calculated rates are listed in the SI (Tables S.7 and S.8, for the MW plasma at reduced and atmospheric pressure, respectively).

In a reduced pressure MW plasma, CH_4 is converted into CH_3 by a combination of electron impact dissociation ($e^- + CH_4 \rightarrow e^- + CH_3 + H$) and reaction with H atoms ($CH_4 + H \rightarrow CH_3 + H_2$). The latter reaction is possible due to the higher temperature in the MW plasma, compared to a DBD, and it is also the main population mechanism of H_2. Some of the CH_3 radicals react back to CH_4 by reactions with C_2H_4 and C_2H_3 ($CH_3 + C_2H_4 \rightarrow CH_4 + C_2H_3$ and $CH_3 + C_2H_3 \rightarrow CH_4 + C_2H_2$). In addition, the CH_3 radicals react further with either CH_3 ($CH_3 + CH_3 + M \rightarrow C_2H_6 + M$, and $CH_3 + CH_3 \rightarrow C_2H_5 + H$) or CH_4 ($CH_4 + CH_3 \rightarrow C_2H_6 + H$), to form both C_2H_6 and C_2H_5. The latter radicals, due to the higher temperature, dissociate mainly further into C_2H_4 ($C_2H_5 + M \rightarrow C_2H_4 + H + M$). However, a small fraction also recombines with CH_3 into C_3H_8 ($CH_3 + C_2H_5 + M \rightarrow C_3H_8 + M$) or with C_2H_5 into C_4H_{10} ($C_2H_5 + C_2H_5 + M \rightarrow C_4H_{10} + M$).
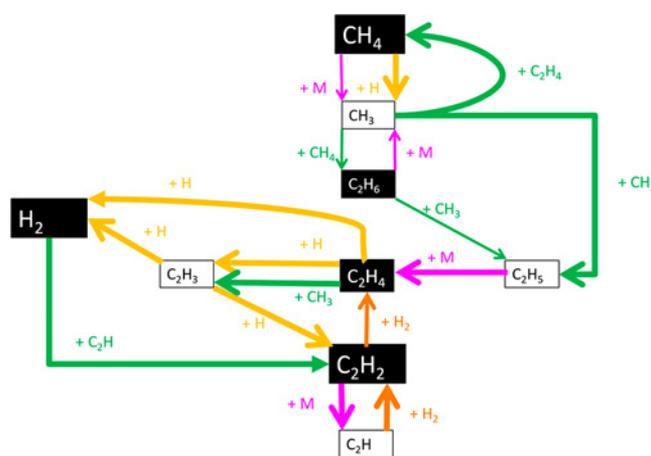
Figure 14. Most important net reaction pathways in a MW plasma at atmospheric pressure. Pink, yellow, green, and orange arrow lines represent reactions involving dissociation with a neutral species M, two-body reactions with H atoms, two-body reactions with hydrocarbon molecules or radicals, and with H_2 molecules, respectively. The thickness of the arrow lines and the size of the boxes are proportional to the reaction rate and species density, respectively as calculated in the model. The black boxes represent stable molecules and the white boxes intermediates (radicals).

C_2H_6 partially dissociates back into CH_3 ($C_2H_6 + M \rightarrow CH_3 + CH_3 + M$), which becomes more important at high SEI values, explaining why high SEI values give lower C_2H_6 selectivities (see Figures 9 and 10). In addition, it also undergoes electron impact dissociation toward C_2H_4 ($e^- + C_2H_6 \rightarrow e^- + C_2H_4 + H_2$), and it reacts with CH_3 or H radicals into C_2H_5 ($CH_3 + C_2H_6 \rightarrow CH_4 + C_2H_5$ and $C_2H_6 + H \rightarrow C_2H_5 + H_2$).

C_2H_4, which is mainly formed by dissociation of C_2H_6 and C_2H_5, reacts mostly further with CH_3 radicals into C_2H_3 ($CH_3 + C_2H_4 \rightarrow CH_4 + C_2H_3$), but a small fraction is also subject to electron impact dissociation, creating C_2H_2 ($e^- + C_2H_4 \rightarrow e^- + C_2H_2 + H_2$), or it reacts with H_2, creating again C_2H_5 ($C_2H_4 + H_2 \rightarrow C_2H_5 + H$).

The C_2H_3 radicals react with CH_3 radicals into either C_3H_6 or C_2H_2, at almost equal rates ($CH_3 + C_2H_3 + M \rightarrow C_3H_6 + M$, and $CH_3 + C_2H_3 \rightarrow CH_4 + C_2H_2$). This is the main formation process of C_3H_6 at high SEI values, while at low SEI values, C_3H_6 is mainly formed by electron impact dissociation of C_3H_8 ($e^- + C_3H_8 \rightarrow e^- + C_3H_6 + H_2$).

At low SEI values, C_3H_6 dissociates mainly into C_2H_2 and C_3H_5 by electron impact dissociation ($e^- + C_3H_6 \rightarrow e^- + C_2H_2 + CH_4$, and $e^- + C_3H_6 \rightarrow e^- + C_3H_5 + H$) and it forms C_3H_7 upon recombination with H atoms ($C_3H_6 + H + M \rightarrow C_3H_7 + M$). At high SEI values, C_3H_6 mainly forms C_3H_5 upon reaction with H or any other neutral molecule ($C_3H_6 + H \rightarrow C_3H_5 + H_2$ and $C_3H_6 + M \rightarrow C_3H_5 + H + M$). C_3H_5 immediately dissociates further into C_2H_2 ($C_3H_5 + M \rightarrow C_2H_2 + CH_3 + M$).

C_3H_8 undergoes electron impact dissociation toward C_3H_6, as mentioned above, but also toward C_2H_4 ($e^- + C_3H_8 \rightarrow e^- + C_2H_4 + CH_4$), and to a smaller extent it reacts with H into C_3H_7 ($C_3H_8 + H \rightarrow C_3H_7 + H_2$). C_3H_7 is formed by dissociation of C_3H_8 and recombination of C_3H_6, as mentioned above, but it is also (and even predominantly) formed by dissociation of C_4H_{10} ($C_4H_{10} + M \rightarrow C_3H_7 + CH_3 + M$). Vice versa, it dissociates into C_2H_4 ($C_3H_7 + M \rightarrow C_2H_4 + CH_3 + M$), thus closing the C_3 and C_4 loop back toward the C_2 hydrocarbons, and explaining why the latter are predominantly formed in MW plasmas.

Finally, C_2H_2, which is the main product at high SEI values, is formed by various electron impact dissociation, neutral dissociation and two-body reactions with several C_2 and C_3 compounds, mainly C_2H_4, C_2H_3, C_3H_6 and C_3H_5, while a small portion reacts further with H_2 toward C_2H_3 ($C_2H_2 + H_2 \rightarrow C_2H_3 + H$), which in turn creates again C_3 compounds, as described above, thus closing the whole cycle.

The chemistry in the atmospheric pressure MW plasma is much less complex, as can be seen in Figure 14. This is attributed to the higher temperature (i.e., >3000 K vs ~2000 K at 30 mbar), causing the dehydrogenation processes to be much more prominent. Like in the reduced pressure case, CH_4 is converted into CH_3, by a combination of electron impact dissociation ($e^- + CH_4 \rightarrow e^- + CH_3 + H$) and reaction with H atoms ($CH_4 + H \rightarrow CH_3 + H_2$). These radicals partially recombine back into CH_4 upon reaction with C_2H_4 ($CH_3 + C_2H_4 \rightarrow CH_4 + C_2H_3$). In addition, they react with CH_4 to produce C_2H_6 ($CH_4 + CH_3 \rightarrow C_2H_6 + H$), which however immediately dissociates back into CH_3 ($C_2H_6 + M \rightarrow CH_3 + CH_3 + M$) or reacts with CH_3 into the formation of C_2H_5 ($CH_3 + C_2H_6 \rightarrow CH_4 + C_2H_5$). Furthermore, two CH_3 radicals also recombine to produce C_2H_5 ($CH_3 + CH_3 \rightarrow C_2H_5 + H$), which immediately dissociates into C_2H_4 ($C_2H_5 + M \rightarrow C_2H_4 + H + M$).

C_2H_4 in turn reacts with CH_3 and H atoms, forming C_2H_3 ($CH_3 + C_2H_4 \rightarrow CH_4 + C_2H_3$ and $C_2H_4 + H \rightarrow C_2H_3 + H_2$), which directly reacts further with H into C_2H_2 ($C_2H_3 + H \rightarrow C_2H_2 + H_2$). Due to the high temperature, C_2H_2 dissociates into C_2H ($C_2H_2 + M \rightarrow C_2H + H + M$), which returns immediately back into C_2H_2 ($C_2H + H_2 \rightarrow C_2H_2 + H$). Finally, a small portion of C_2H_2 also recombines back with H_2 into the formation of C_2H_4 ($C_2H_2 + H_2 + M \rightarrow C_2H_4 + M$), closing the loop. Although H_2 is a reactant, it is immediately formed again by the dehydrogenation processes, forming ultimately C_2H_2.

The reaction pathways in Figures 13 and 14 mainly exhibit thermal reactions, with some contribution of electron impact dissociation at reduced pressure (Figure 13). This is of course due to the high temperature, enabling these thermal reactions, in contrast with the DBD, where electron impact dissociation and also ionization were much more predominant (Figure 8). Lower pressures and lower powers furthermore favor recombination processes, resulting in the formation of C_3 compounds. Higher pressures and higher powers induce dehydrogenation reactions, resulting in more unsaturated hydrocarbons, and thus explaining the high C_2H_2 selectivity in Figures 10−12.

In addition, we investigated the role of vibrational-induced dissociation of CH_4 in the MW plasma, as this process is important in the case of CO_2 splitting and N_2 fixation,[46−49] especially in low pressure MW plasmas, where there is a pronounced vibrational−translational nonequilibrium. For this purpose, we calculated the vibrational temperature, from the four vibrational levels included in our model:

$$T_v = \frac{1}{4} \sum_{i=1}^{4} -\frac{E_i}{\log\left(\frac{n_i}{g_i n_o}\right)} \tag{10}$$

with E_i the energy of the first level of vibrational mode v_i of CH_4 (in K), g_i its degeneracy and n_i its density (in cm^{-3}). n_o is the density of ground state CH_4.

We found that, for the MW plasma conditions in this study, the vibrational temperature of CH_4 is almost equal to the gas temperature, indicating that the vibration-translational nonequilibrium in CH_4 MW plasma is negligible, even at reduced pressure (see Figures S.7 and S.8 in the Supporting Information). This finding is supported by measurements of Butterworth et al.[50]

3.3. GAP. *3.3.1. Comparison of Calculated and Measured CH_4 Conversion, Energy Costs, and Product Selectivities.* The experimental and calculated CH_4 conversions, energy costs and selectivities of the most important hydrocarbons and H_2 are plotted in Figure 15 as a function of CH_4 fraction in the CH_4/N_2
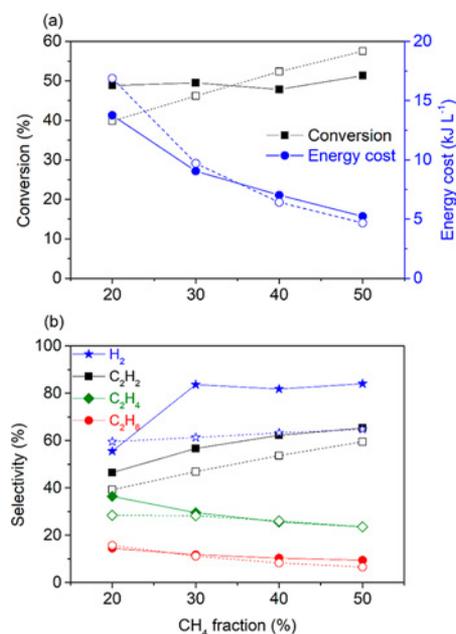
Figure 15. Calculated (dashed lines) and experimental (solid lines) CH_4 conversions and energy costs (a), as well as selectivities of the most important hydrocarbons and H_2 formed (b), in the GAP, as a function of CH_4 fraction in the CH_4/N_2 mixture, for an input power of 224 W and a flow rate of 10 L min^{-1}.

mixture, at a power of 224 W and a flow rate of 10 L min^{-1}. The agreement is very reasonable, with a maximum discrepancy between the experimental and calculated results of 36% for the C_2H_6 selectivity (at a CH_4 fraction of 50%) and an average discrepancy of 15%. In addition, both experimental and calculated results follow the same trends as a function of CH_4 fraction. Therefore, we believe our model can provide a reasonable description of the chemistry inside the GAP, operating in CH_4/N_2 at various mixing ratios.

The conversion is around 50%, and the energy cost is between 5 and 15 kJ L^{-1}, decreasing for higher CH_4 fraction in the mixture. This is significantly lower than the energy costs obtained in the DBD and in the MW plasma, both at reduced and atmospheric pressure. The fact that the energy cost is much lower than in a DBD is not surprising, as this is also the case for other gas conversion processes, such as CO_2 splitting, dry reforming of methane, and N_2 fixation.[6,51] However, the fact that it is also clearly lower than the MW plasma is quite striking, as both plasma sources operate at similar temperature (>3000 K) and power (>200 W). On the other hand, the flow rate in the GAP (10 L min^{-1}) is much higher than in the MW plasma (100−1000 mL min^{-1}), so the SEI in the GAP is much lower, demonstrating the superior performance in terms of energy cost.

The most important product formed is C_2H_2 (with selectivities ranging between 46% and 65%), followed by

C_2H_4 (with selectivities between 24% and 36%) and finally C_2H_6 (with selectivities between 9% and 15%).

3.3.2. Underlying Reaction Pathways. The underlying reaction mechanisms in the GAP are presented in Figure 16.
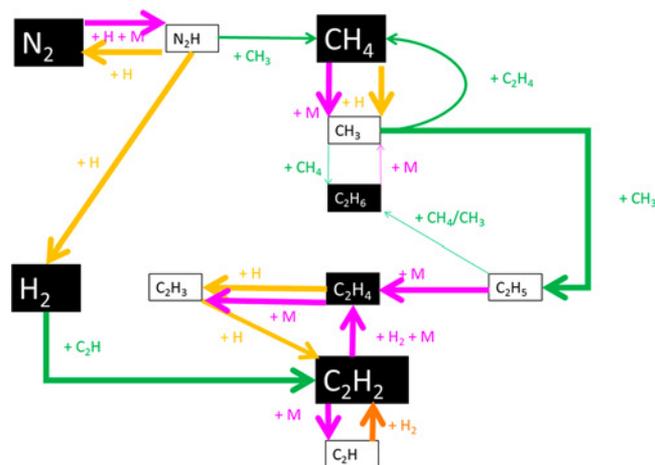
Figure 16. Most important net reaction pathways in the GAP at atmospheric pressure. Pink, yellow, green, and orange arrow lines represent reactions involving a neutral species M in three-body reactions or neutral dissociation, two-body reactions with H atoms, two-body reactions with hydrocarbon molecules or radicals, and with H_2 molecules, respectively. The thickness of the arrow lines and the size of the boxes are proportional to the reaction rate and species density, respectively, as calculated by the model. The black boxes represent stable molecules and the white boxes intermediates (radicals).

They are similar as in the MW plasma at atmospheric pressure, which is logical, because both plasma types operate at similar temperatures and powers, as mentioned above. The calculated rates of the reactions in this figure are listed in the SI (Table S.9).

Just as in the MW plasma at atmospheric pressure, CH_4 is converted into CH_3 radicals upon both neutral dissociation ($CH_4 + M \rightarrow CH_3 + H + M$) and reaction with H atoms ($CH_4 + H \rightarrow CH_3 + H_2$). The CH_3 radicals partially react with C_2H_4 to form CH_4 again ($CH_3 + C_2H_4 \rightarrow CH_4 + C_2H_3$) but also with N_2H ($CH_3 + N_2H \rightarrow CH_4 + N_2$), the latter being formed by N_2 reacting with H atoms ($N_2 + H + M \rightarrow N_2H + M$). Finally, some CH_3 radicals also form C_2H_6 ($CH_4 + CH_3 \rightarrow C_2H_6 + H$), which however immediately dissociates back into CH_3 ($C_2H_6 + M \rightarrow CH_3 + CH_3 + M$) or reacts with CH_3 into the formation of C_2H_5 ($CH_3 + C_2H_6 \rightarrow CH_4 + C_2H_5$).

The rest of the pathways is identical to the atmospheric MW plasma, with the exception that C_2H_5 partially reacts back to C_2H_6 ($CH_3 + C_2H_5 \rightarrow C_2H_6 + CH_2$, and $CH_4 + C_2H_5 \rightarrow CH_3 + C_2H_6$) and C_2H_4 also dissociates in C_2H_3 using neutral dissociation ($C_2H_4 + M \rightarrow C_2H_3 + H + M$) due to the higher temperatures in the GAP, especially in the beginning of the arc discharge near the cathode spot.

Thus, dehydrogenation and neutral dissociation reactions of the produced hydrocarbons are the most important processes in the GAP, resulting especially in the formation of C_2H_2.

The fact that the majority of CH_4 dissociates in the GAP, even at the high flow rate of 10 L min^{-1} (which is at least a factor 10 higher than in the MW plasma at atmospheric pressure, cf. Figure 12; and even up to 3 orders of magnitude higher than in the DBD; cf. Figures 4−7), point toward the high efficiency of the GAP for CH_4 conversion, compared to the MW and DBD plasmas. This is attributed to the high temperature of the GAP, favoring thermal CH_4 dissociation.

In terms of energy cost, we can conclude that sufficiently high temperatures to induce thermal dissociation, together with a high flow rate, are needed for CH_4 conversion at low energy cost. Indeed, our model predicts that also in the GAP, vibration-induced dissociation of CH_4 is negligible, and there is no vibrational−translational nonequilibrium. In addition, mainly C_2H_2 and H_2 are formed, next to C_2H_4. It would be even more beneficial if the selectivity toward C_2H_4 could be enhanced, to make plasma technology of interest for the production of this important chemical compound, and thus for electrification of the chemical industry.[52] Note that the C_2H_4 selectivity could be enhanced by introducing a catalyst after the plasma reactor, to convert the produced C_2H_2 into C_2H_4, as demonstrated by Delikonstantis et al.[53]

3.4. Plasma vs Thermal Conversion. It is clear from previous sections that the higher temperature of MW and GA plasma leads to higher conversion and more selective production of unsaturated hydrocarbons. To investigate whether the conversion in these plasmas is purely thermal or due to (additional) plasma effects, we make a distinction between the plasma effects and the thermal effects for the same range of conditions as investigated in sections 3.2 and 3.3.

Figure 17 shows the CH_4 conversions for the MW plasma at reduced pressure (30 mbar), obtained in the plasma and by pure thermal conversion at the same temperature (i.e., without electron impact reactions, which are specific plasma-based reactions), as a function of SEI, for the continuous (a) and pulsed (b) regime. The corresponding gas temperature is
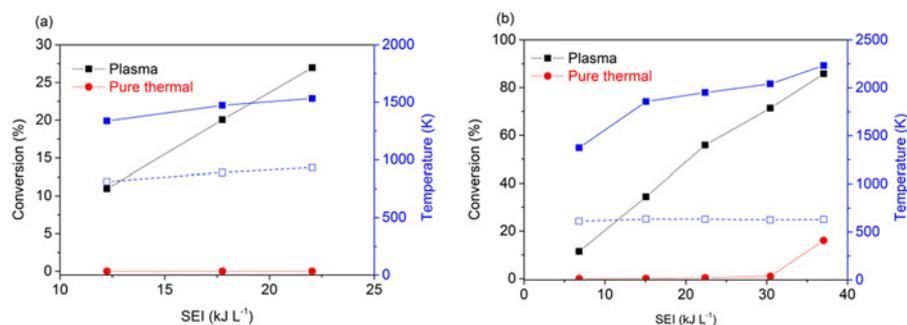
Figure 17. Calculated conversion by the plasma and by pure thermal conversion (i.e., without electron impact reactions; left *y*-axis), as well as calculated maximum gas temperature inside the plasma/pulses (solid line) and averaged over the whole residence time in the reactor (dashed line; right *y*-axis), as a function of SEI, in a MW plasma at a pressure of 30 mbar and flow rate of 98 sccm, operating in a continuous (a) and pulsed (b) regime.
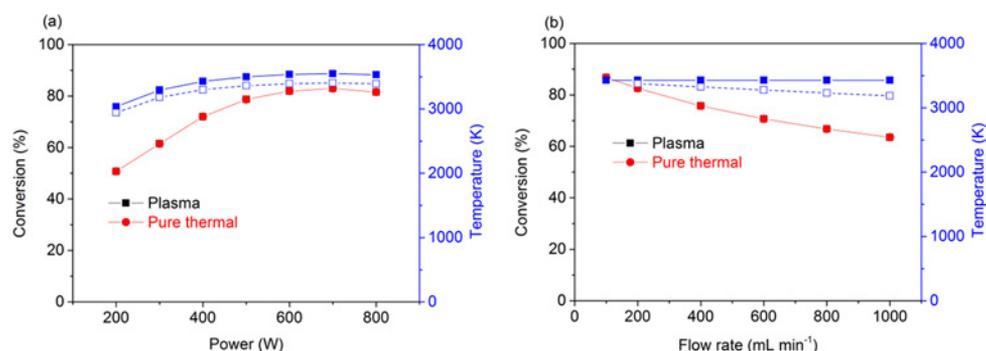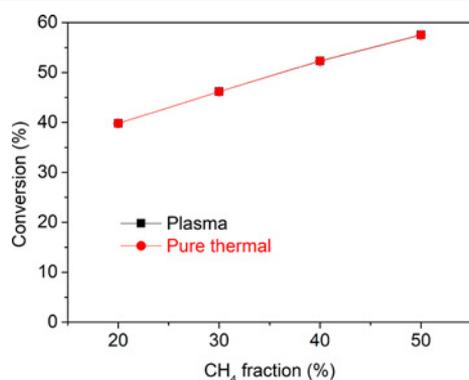
Figure 18. Calculated conversion by the plasma and by pure thermal conversion (i.e., without electron impact reactions) (left *y*-axis), as well as calculated maximum gas temperature (solid line) and averaged over the whole residence time in the reactor (dashed line) (right *y*-axis), as a function of microwave power, at a flow rate of 500 mL min^{-1} (a), and as a function of flow rate, at a microwave power of 400 W (b), in an atmospheric pressure MW plasma, for a CH$_4$/H$_2$ ratio of 1/4. Note that the plasma conversion and pure thermal conversion perfectly overlap.

plotted in blue color (right *y*-axis). Both the maximum temperature and averaged temperature (obtained by averaging over the whole residence time) are plotted. At this reduced pressure, almost all conversion is due to plasma effects. Indeed, despite the fact that the maximum temperatures obtained in both the continuous and pulsed mode can reach 1500 K and more, which is in principle sufficient to induce significant thermal conversion, this temperature is only reached for a short time, even in the continuous mode, due to the triangular power profile, as explained in section 1.7 in the SI ($\sim$30 μs in the pulsed mode and $\sim$100 μs in the continuous mode), causing the average temperature in the MW plasma to be too low for thermal conversion. During the short plasma time, however, enough reactive species are created, which, due to the higher local temperatures, react further in neutral reactions. These reactive species are mainly CH$_3$ and H, as can be seen in Figure 13, and are mainly created by electron impact dissociation of CH$_4$ or neutral dissociation of higher hydrocarbons, as illustrated in Figures S.12 and S.13 in the SI.

However, in the atmospheric pressure MW plasma and in the GAP discharge, the conversions obtained with and without electron impact reactions are virtually the same, as is clear from Figures 18 and 19, indicating that the conversion is purely thermal at the high temperatures of 3000–3500 K. However, plasmas can still be beneficial above classical thermal conversion,
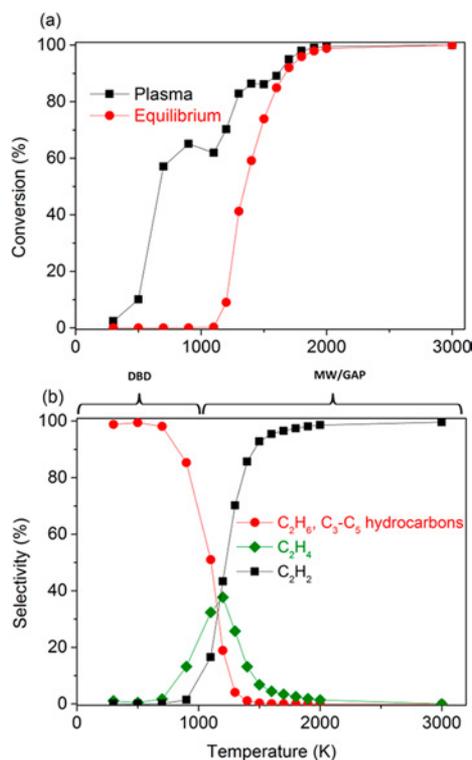

Figure 19. Calculated conversion by the plasma and by pure thermal conversion (i.e., without electron impact reactions) in the GAP, as a function of CH$_4$ fraction in the CH$_4$/N$_2$ mixture, for an input power of 224 W and a flow rate of 10 L min^{-1}. The plasma conversion and pure thermal conversion perfectly overlap. The used temperature profile for all conditions studied can be seen in Figure S.1 in the SI.

as high temperatures (3000–3500 K) can be reached by applying electric power (of interest for electrification of chemical reactions) and without damaging the reactor. Indeed, the arc in the GAP can be easily contained in the reactor center due to the reverse vortex flow, which isolates the hot plasma from the reactor walls[54] and in MW plasmas at atmospheric pressure, gas contraction takes place, also focusing the plasma in the center, and thus also protecting the reactor walls.[55,56] Finally, plasmas can be switched on and off quite fast, with ignition times equal to several 100 ms in plasma torches,[57] making them compatible with fluctuating renewable electricity.

Besides the gas temperature, also the electron density is completely different in the three different plasma types. In the DBD plasma the electron densities are calculated to be between 5×10^{13} cm^{-3} and 2×10^{14} cm^{-3}. In the MW plasma at reduced pressure, the electron densities range between 1.6×10^{12} and 2.4×10^{13} cm^{-3}, while in the MW plasma at atmospheric pressure, the electron densities vary between 6.0×10^{11} and 1.4×10^{12} cm^{-3}. Finally, in the GAP the electron density is calculated to be $\sim$6.0 $\times 10^{11}$ cm^{-3}. Thus, the calculated electron density is the highest in the DBD, more specifically inside the filaments. Combined with the low gas temperature (<500 K), it is logical that electron impact reactions, next to three-body recombinations, are dominant. Since a 0D model cannot capture spatial nonuniformities, such as plasma contraction, local higher power densities may be underestimated, which might result in lower electron densities. Nevertheless, since the gas temperatures are around 3000 K or higher in the (atmospheric pressure) MW plasma and the GAP, CH$_4$ dissociates very fast at these temperatures, so we are confident that our conclusion about the importance of thermal conversion is valid, even if the electron densities would be somewhat underestimated.

To assess whether temperature controls the overall chemical behavior, we plot in Figure 20a,b the CH$_4$ conversion and product selectivities for a generic type of plasma, at 400 W and a flow rate of 500 mL min^{-1}, as a function of gas temperature. It is clear that the temperature indeed plays a determining role in steering the conversion and the product selectivities. Gas temperatures below 1000 K favor radical recombination processes, resulting in more saturated hydrocarbons (C$_2$H$_6$ and higher C$_3$–C$_5$ hydrocarbons), as demonstrated in section 3.1.2 for DBD plasmas. Higher temperatures favor neutral dissociation and dehydrogenation, explaining why C$_2$H$_4$ and especially C$_2$H$_2$ are the dominant products in the MW plasma and the GAP.

Figure 20. Calculated conversion (a) and most important hydrocarbon selectivities (b) inside a generic plasma type at atmospheric pressure, a power of 400 W and a flow rate of 500 mL min^{-1} for pure CH_4, as a function of gas temperature. In (a) both the plasma conversion and thermal equilibrium conversion are plotted, indicating a clear difference up to 2000 K.

In Figure 20a we also compare the plasma conversion and conversion at thermal equilibrium, demonstrating that up to a temperature of 2000 K, there is still a significant difference. Hence, the plasma effect can still be important in warm plasmas at atmospheric pressure, when the temperature would be below 2000 K. However, for the atmospheric pressure MW plasma and GAP studied in sections 3.2 and 3.3 above, the gas temperature is around 3000 K or above, and the conversion occurs by thermal processes.

4. CONCLUSIONS

CH_4 conversion into higher hydrocarbons and H_2 by plasma technology is gaining increasing interest as more sustainable alternative to conventional steam reforming. However, different plasma types yield a different performance in terms of conversion, energy cost and selectivity toward different hydrocarbons, and the underlying mechanisms are not yet fully understood. Therefore, we developed a chemical kinetics model to elucidate the main conversion mechanisms of CH_4 into the most important hydrocarbons, especially C_2H_2, C_2H_4 and C_2H_6, as well as into H_2, in the three most commonly used plasma reactors, i.e., a DBD, MW, and GAP reactor. We first compared the calculated conversions, energy costs and product selectivities with experimental results in different reactor configurations and in a wide range of operating conditions. The calculation results are in satisfactory agreement with the experiments, which indicates that our model can provide a realistic picture of the underlying chemistry in CH_4 plasmas and even CH_4–H_2-N_2 mixtures, and can be used to elucidate the

underlying mechanisms of CH_4 conversion into various hydrocarbons and H_2 in the different plasma reactors.

The CH_4 conversion is around 20% in the DBD, as well as in the MW plasma at reduced pressure, but it rises to values above 80% in the pulsed MW plasma, as well as at atmospheric pressure, both upon rising SEI. In the GAP, conversions around 50% were obtained, even at high flow rates of 10 L min^{-1}. Because of this high flow rate, the GAP operates at much lower SEI than the other plasma sources, i.e., around 1.3 kJ L^{-1}, vs 9–54 kJ L^{-1} for the DBD, 7–37 kJ L^{-1} for the reduced pressure MW plasma, and 24–240 kJ L^{-1} for the atmospheric pressure MW plasma. Therefore, the corresponding energy cost is by far the lowest for the GAP (between 5 and 15 kJ/L, decreasing upon higher CH_4 fraction in the mixture), while it is around 40–140 kJ L^{-1} in the reduced pressure MW plasma, from 200 until above 1000 kJ L^{-1} in the atmospheric pressure MW plasma, and around 125–510 kJ L^{-1} in the DBD. As the GAP operates at the highest temperatures, this illustrates that thermal CH_4 conversion is important, and most efficient. Indeed, our model predicts that vibrational–translational nonequilibrium is negligible in all these CH_4 plasmas.

We can conclude that higher temperatures, especially in the GAP but also in atmospheric pressure MW plasmas, result in more CH_4 conversion, and in neutral dissociation and dehydrogenation processes of the hydrocarbons created, forming especially C_2H_2 and H_2, and (some) C_2H_4. Low temperature plasmas, such as DBD and reduced pressure MW plasmas, result in more electron impact dissociation and three-body recombination processes, creating more saturated compounds, i.e., mainly C_2H_6, but also higher hydrocarbons, such as C_3H_8 and C_4H_{10}.

Thus, high temperature plasmas, and especially the GAP, which operates at high flow rates, are clearly beneficial, for both higher and more energy-efficient CH_4 conversion, as well as more selective production of C_2H_2 and (to a lower extent) C_2H_4. It would even be better if C_2H_4 would be the major product. To realize this, it is possible to add a catalyst after the plasma reactor, to convert C_2H_2 into C_2H_4, as demonstrated by Delikonstantis et al. for a nanosecond pulsed plasma.[53] This will be the subject of our future work.

■ ASSOCIATED CONTENT

ⓢ Supporting Information

The Supporting Information is available free of charge at https://pubs.acs.org/doi/10.1021/acs.jpcc.0c00082.

> Full description of the 0D model, including the vibrational and rotational kinetics of CH_4 and the vibrational kinetics of H_2, and a list of all reactions included in the model for the CH_4 and CH_4-N_2 chemistry. In addition, details are given on the assumptions made to describe the DBD, MW plasma and GAP, as well as about the experiments performed in the GAP. We also present additional calculation results, i.e., the vibrational and gas temperature in the different plasma sources, to demonstrate that the various CH_4 plasmas investigated are close to vibrational–translational equilibrium. Finally, we present the calculated rates of the most important reactions in the various plasma sources, to identify the reaction pathways plotted in Figures 8, 13, 14 and 16 and the net contribution of the most important formation mechanisms of H and CH_3 in the reduced pressure MW discharge. (PDF)

■ AUTHOR INFORMATION

Corresponding Authors

    Stijn Heijkers — *Research group PLASMANT, Department of Chemistry, University of Antwerp BE-2610 Wilrijk-Antwerp, Belgium;* ⊙ orcid.org/0000-0001-7142-9697; Phone: +3232652369; Email: stijn.heijkers@uantwerpen.be

    Annemie Bogaerts — *Research group PLASMANT, Department of Chemistry, University of Antwerp BE-2610 Wilrijk-Antwerp, Belgium;* ⊙ orcid.org/0000-0001-9875-6460; Phone: +3232652377; Email: annemie.bogaerts@uantwerpen.be

Author

    Maryam Aghaei — *Research group PLASMANT, Department of Chemistry, University of Antwerp BE-2610 Wilrijk-Antwerp, Belgium;* ⊙ orcid.org/0000-0003-4995-8773

Complete contact information is available at:
https://pubs.acs.org/10.1021/acs.jpcc.0c00082

Notes

The authors declare no competing financial interest.

■ REFERENCES

(1) Van Geem, K. M.; Galvita, V. V.; Marin, G. B. Making Chemicals with Electricity. *Science (Washington, DC, U. S.)* **2019**, *364*, 734−735.

(2) Bellussi, G.; Pollesel, P. Industrial Applications of Zeolite Catalysis: Production and Uses of Light Olefins. *Stud. Surf. Sci. Catal.* **2005**, *158*, 1201−1212.

(3) Hoveyda, A. H.; Zhugralin, A. R. The Remarkable Metal-Catalysed Olefin Metathesis Reaction. *Nature* **2007**, *450*, 243−251.

(4) Holmen, A.; Olsvik, O.; Rokstad, O. A. Pyrolysis of Natural Gas: Chemistry and Process Concepts. *Fuel Process. Technol.* **1995**, *42*, 249−267.

(5) Scapinello, M.; Delikonstantis, E.; Stefanidis, G. D. The Panorama of Plasma-Assisted Non-Oxidative Methane Reforming. *Chem. Eng. Process.* **2017**, *117*, 120−140.

(6) Snoeckx, R.; Bogaerts, A. Plasma Technology-a Novel Solution for CO_2 Conversion? *Chem. Soc. Rev.* **2017**, *46*, 5805−5863.

(7) Kasinathan, P.; Park, S.; Choi, W. C.; Hwang, Y. K.; Chang, J. S.; Park, Y. K. Plasma-Enhanced Methane Direct Conversion over Particle-Size Adjusted MO_x/Al_2O_3(M = Ti and Mg) Catalysts. *Plasma Chem. Plasma Process.* **2014**, *34*, 1317−1330.

(8) Lü, J.; Li, Z. Conversion of Natural Gas to C_2 Hydrocarbons via Cold Plasma Technology. *J. Nat. Gas Chem.* **2010**, *19*, 375−379.

(9) Li, X. S.; Zhu, A. M.; Wang, K. J.; Xu, Y.; Song, Z. M. Methane Conversion to C_2 Hydrocarbons and Hydrogen in Atmospheric Non-Thermal Plasmas Generated by Different Electric Discharge Techniques. *Catal. Today* **2004**, *98*, 617−624.

(10) Xu, C.; Tu, X. Plasma-Assisted Methane Conversion in an Atmospheric Pressure Dielectric Barrier Discharge Reactor. *J. Energy Chem.* **2013**, *22*, 420−425.

(11) Zhang, H.; Du, C.; Wu, A.; Bo, Z.; Yan, J.; Li, X. Rotating Gliding Arc Assisted Methane Decomposition in Nitrogen for Hydrogen Production. *Int. J. Hydrogen Energy* **2014**, *39*, 12620−12635.

(12) Heintze, M.; Magureanu, M. Methane Conversion into Acetylene in a Microwave Plasma: Optimization of the Operating Parameters. *J. Appl. Phys.* **2002**, *92* (5), 2276−2283.

(13) Cho, W.; Kim, Y. C.; Kim, S. S. Conversion of Natural Gas to C_2 Product, Hydrogen and Carbon Black Using a Catalytic Plasma Reaction. *J. Ind. Eng. Chem.* **2010**, *16*, 20−26.

(14) Shen, C.; Sun, D.; Yang, H. Methane Coupling in Microwave Plasma under Atmospheric Pressure. *J. Nat. Gas Chem.* **2011**, *20*, 449−456.

(15) Młotek, M.; Sentek, J.; Krawczyk, K.; Schmidt-Szałowski, K. The Hybrid Plasma-Catalytic Process for Non-Oxidative Methane Coupling to Ethylene and Ethane. *Appl. Catal., A* **2009**, *366*, 232−241.

(16) Yuhan, Z. Methane Pyrolysis to Acetylene in Gliding Arc Plasma Driven by Magnetism. *Proc. - Int. Conf. Comput. Distrib. Control Intell. Environ. Monit. CDCIEM 2011* **2011**, *2*, 894−896.

(17) Lee, H.; Sekiguchi, H. Plasma-Catalytic Hybrid System Using Spouted Bed with a Gliding Arc Discharge: CH_4 Reforming as a Model Reaction. *J. Phys. D: Appl. Phys.* **2011**, *44*, 274008.

(18) Polak, L. S. Low-Temperature Plasma in Petroleum Chemistry. *Pet. Chem. U.S.S.R* **1967**, *7*, 136−152.

(19) Indarto, A.; Coowanitwong, N.; Choi, J. W.; Lee, H.; Song, H. K. Kinetic Modeling of Plasma Methane Conversion in a Dielectric Barrier Discharge. *Fuel Process. Technol.* **2008**, *89*, 214−219.

(20) De Bie, C.; Verheyde, B.; Martens, T.; Van Dijk, J.; Paulussen, S.; Bogaerts, A. Fluid Modeling of the Conversion of Methane into Higher Hydrocarbons in an Atmospheric Pressure Dielectric Barrier Discharge. *Plasma Processes Polym.* **2011**, *8*, 1033−1058.

(21) Istadi, I.; Amin, N. A. S. Modelling and Optimization of Catalytic-Dielectric Barrier Discharge Plasma Reactor for Methane and Carbon Dioxide Conversion Using Hybrid Artificial Neural Network-Genetic Algorithm Technique. *Chem. Eng. Sci.* **2007**, *62* (23), 6568−6581.

(22) Yang, Y. Direct Non-Oxidative Methane Conversion by Non-Thermal Plasma: Modeling Study. *Plasma Chem. Plasma Process.* **2003**, *23*, 327−346.

(23) Dors, M.; Nowakowska, H.; Jasiński, M.; Mizeraczyk, J. Chemical Kinetics of Methane Pyrolysis in Microwave Plasma at Atmospheric Pressure. *Plasma Chem. Plasma Process.* **2014**, *34*, 313−326.

(24) Indarto, A.; Choi, J. W.; Lee, H.; Song, H. K. Kinetic Modeling of Plasma Methane Conversion Using Gliding Arc. *J. Nat. Gas Chem.* **2005**, *14*, 13−21.

(25) Hassouni, K.; Duten, X.; Rousseau, A.; Gicquel, A. Investigation of Chemical Kinetics and Energy Transfer in a Pulsed Microwave H_2/CH_4 Plasma. *Plasma Sources Sci. Technol.* **2001**, *10*, 61−75.

(26) Lombardi, G.; Hassouni, K.; Stancu, G. D.; Mechold, L.; Röpcke, J.; Gicquel, A. Study of an H_2/CH_4 Moderate Pressure Microwave Plasma Used for Diamond Deposition: Modelling and IR Tuneable Diode Laser Diagnostic. *Plasma Sources Sci. Technol.* **2005**, *14*, 440−450.

(27) Snoeckx, R.; Aerts, R.; Tu, X.; Bogaerts, A. Plasma-Based Dry Reforming: A Computational Study Ranging from the Nanoseconds to Seconds Time Scale. *J. Phys. Chem. C* **2013**, *117*, 4957−4970.

(28) Cleiren, E.; Heijkers, S.; Ramakers, M.; Bogaerts, A. Dry Reforming of Methane in a Gliding Arc Plasmatron: Towards a Better Understanding of the Plasma Chemistry. *ChemSusChem* **2017**, *10*, 4025−4036.

(29) Pancheshnyi, S.; Eismann, B.; Hagelaar, G. J. M.; Pitchford, L. C. *ZDPlasKin: A New Tool for Plasmachemical Simulations*; University of Toulouse, LAPLACE, CNRS-UPS-INP: Toulouse, France, 2008.

(30) Hagelaar, G. J. M.; Pitchford, L. C. Solving the Boltzmann Equation to Obtain Electron Transport Coefficients and Rate Coefficients for Fluid Models. *Plasma Sources Sci. Technol.* **2005**, *14*, 722−733.

(31) Kozak, T.; Bogaerts, A. Evaluation of the Energy Efficiency of CO_2 Conversion in Microwave Discharges Using a Reaction Kinetics Model. *Plasma Sources Sci. Technol.* **2015**, *24*, 015024.

(32) Wang, B.; Yan, W.; Ge, W.; Duan, X. Methane Conversion into Higher Hydrocarbons with Dielectric Barrier Discharge Micro-Plasma Reactor. *J. Energy Chem.* 2013, 22, 876−882.

(33) Ozkan, A.; Dufour, T.; Silva, T.; Britun, N.; Snyders, R.; Reniers, F.; Bogaerts, A. DBD in Burst Mode : Solution for More Efficient CO_2 Conversion ? *Plasma Sources Sci. Technol.* 2016, 25, 055005.

(34) Ozkan, A.; Dufour, T.; Bogaerts, A.; Reniers, F. How Do the Barrier Thickness and Dielectric Material Influence the Filamentary Mode and CO_2 Conversion in a Flowing DBD? *Plasma Sources Sci. Technol.* 2016, 25, 045016.

(35) Fridman, A. *Plasma Chemistry*; Cambridge University Press: New York, 2008.

(36) Papageorghiou, L.; Panousis, E.; Loiseau, J. F.; Spyrou, N.; Held, B. Two-Dimensional Modelling of a Nitrogen Dielectric Barrier Discharge (DBD) at Atmospheric Pressure: Filament Dynamics with the Dielectric Barrier on the Cathode. *J. Phys. D: Appl. Phys.* 2009, 42, 105201.

(37) Snoeckx, R.; Heijkers, S.; Van Wesenbeeck, K.; Lenaerts, S.; Bogaerts, A. CO_2 Conversion in a Dielectric Barrier Discharge Plasma: N_2 in the Mix as a Helping Hand or Problematic Impurity? *Energy Environ. Sci.* 2016, 9, 30−39.

(38) Kuznetsova, I. V.; Kalashnikov, N. Y.; Gutsol, a. F.; Fridman, a. a.; Kennedy, L. a. Effect of "Overshooting" in the Transitional Regimes of the Low-Current Gliding Arc Discharge. *J. Appl. Phys.* 2002, 92 (8), 4231−4237.

(39) Nunnally, T. P. *Application of Low Current Gliding Arc Plasma Discharges for Hydrogen Sulfide Decomposition and Carbon Dioxide Emission Reduction.* Ph.D. Dissertation; Drexel University, 2011.

(40) Nunnally, T.; Gutsol, K.; Rabinovich, A.; Fridman, A.; Gutsol, A.; Kemoun, A. Dissociation of CO_2 in a Low Current Gliding Arc Plasmatron. *J. Phys. D: Appl. Phys.* 2011, 44, 274009.

(41) Ramakers, M.; Trenchev, G.; Heijkers, S.; Wang, W.; Bogaerts, A. Gliding Arc Plasmatron: Providing a Novel Method for Carbon Dioxide Conversion. *ChemSusChem* 2017, 10, 2642−2652.

(42) Ramakers, M.; Heijkers, S.; Tytgat, T.; Lenaerts, S.; Bogaerts, A. Combining CO_2 Conversion and N_2 Fixation in a Gliding Arc Plasmatron. *J. CO2 Util.* 2019, 33, 121−130.

(43) Trenchev, G.; Kolev, S.; Bogaerts, A. A 3D Model of a Reverse Vortex Flow Gliding Arc Reactor. *Plasma Sources Sci. Technol.* 2016, 25 (3), 035014.

(44) Trenchev, G.; Kolev, S.; Wang, W.; Ramakers, M.; Bogaerts, A. CO_2 Conversion in a Gliding Arc Plasmatron: Multidimensional Modeling for Improved Efficiency. *J. Phys. Chem. C* 2017, 121 (44), 24470−24479.

(45) Heijkers, S.; Bogaerts, A. CO_2 Conversion in a Gliding Arc Plasmatron: Elucidating the Chemistry through Kinetic Modeling. *J. Phys. Chem. C* 2017, 121, 22644−22655.

(46) Kozák, T.; Bogaerts, A. Splitting of CO_2 by Vibrational Excitation in Non-Equilibrium Plasmas: A Reaction Kinetics Model. *Plasma Sources Sci. Technol.* 2014, 23, 045004.

(47) Berthelot, A.; Bogaerts, A. Modeling of CO_2 Splitting in a Microwave Plasma: How to Improve the Conversion and Energy Efficiency. *J. Phys. Chem. C* 2017, 121 (15), 8236−8251.

(48) Vermeiren, V.; Bogaerts, A. Supersonic Microwave Plasma: Potential and Limitations for Energy-Efficient CO_2 Conversion. *J. Phys. Chem. C* 2018, 122, 25869−25881.

(49) Van Alphen, S.; Vermeiren, V.; Butterworth, T.; Van Den Bekerom, D. C. M.; Van Rooij, G. J.; Bogaerts, A. Power Pulsing to Maximize Vibrational Excitation Efficiency in N2Microwave Plasma: A Combined Experimental and Computational Study. *J. Phys. Chem. C* 2020, 124, 1765.

(50) Butterworth, T. D.; Amyay, B.; Bekerom, D. V.D.; Steeg, A. V.D.; Minea, T.; Gatti, N.; Ong, Q.; Richard, C.; van Kruijsdijk, C.; Smits, J. T.; et al. Quantifying Methane Vibrational and Rotational Temperature with Raman Scattering. *J. Quant. Spectrosc. Radiat. Transfer* 2019, 236, 106562.

(51) Bogaerts, A.; Neyts, E. C. Plasma Technology: An Emerging Technology for Energy Storage. *ACS Energy Lett.* 2018, 3, 1013−1027.

(52) Schiffer, Z. J.; Manthiram, K. Electrification and Decarbonization of the Chemical Industry. *Joule* 2017, 1, 10−14.

(53) Delikonstantis, E.; Scapinello, M.; Stefanidis, G. D. Low Energy Cost Conversion of Methane to Ethylene in a Hybrid Plasma-Catalytic Reactor System. *Fuel Process. Technol.* 2018, 176, 33−42.

(54) Kalra, C. S.; Cho, Y. I.; Gutsol, A.; Fridman, A.; Rufael, T. S. Gliding Arc in Tornado Using a Reverse Vortex Flow. *Rev. Sci. Instrum.* 2005, 76 (2), 025110.

(55) Kabouzi, Y.; Calzada, M. D.; Moisan, M.; Tran, K. C.; Trassy, C. Radial Contraction of Microwave-Sustained Plasma Columns at Atmospheric Pressure. *J. Appl. Phys.* 2002, 91, 1008−1019.

(56) den Harder, N.; van den Bekerom, D. C. M.; Al, R. S.; Graswinckel, M. F.; Palomares, J. M.; Peeters, F. J. J.; Ponduri, S.; Minea, T.; Bongers, W. A.; van de Sanden, M. C. M.; et al. Homogeneous CO_2 Conversion by Microwave Plasma: Wave Propagation and Diagnostics. *Plasma Process. Polym.* 2017, 14, e1600120.

(57) Cao, X.; Yu, D.; Xiang, Y.; Li, C.; Jiang, H.; Yao, J. Study on the Ignition Process of a Segmented Plasma Torch. *Plasma Sci. Technol.* 2017, 19, 075404.